

Electronic Supplementary Information (ESI) for

Valence-shell photoelectron circular dichroism of ruthenium(III)-tris-(acetylacetonato) gas-phase enantiomers

Benoît Darquié,^{*a} Nidal Saleh,^{b,c} Sean K. Tokunaga,^a Monika Srebro-Hooper,^{*d} Aurora Ponzi,^{e,f} Jochen Autschbach,^g Piero Decleva,^{*e} Gustavo A. Garcia,^h Jeanne Crassous,^{*b} Laurent Nahon^{*h}

^a Laboratoire de Physique des Lasers, Université Sorbonne Paris Nord, CNRS, Villetaneuse, France.

Email: benoit.darquie@univ-paris13.fr.

^b Univ Rennes CNRS, ISCR—UMR 6226 ScanMat – UMS 2001, 35000 Rennes, France.

Email: jeanne.crassous@univ-rennes1.fr.

^c Current address: Department of Organic Chemistry, University of Geneva, Quai Ernest Ansermet 30, 1211 Geneva 4, Switzerland.

^d Faculty of Chemistry, Jagiellonian University, Gronostajowa 2, 30-387 Krakow, Poland.

Email: srebro@chemia.uj.edu.pl.

^e CNR IOM and Dipartimento di Scienze Cghimiche e Farmaceutiche, Universita' di Trieste, I-34127 Trieste, Italy.

Email: decleva@units.it.

^f Current address: Department of Physical Chemistry, Ruder Bošković Institute, 10000 Zagreb, Croatia.

^g Department of Chemistry, University at Buffalo, State University of New York, Buffalo, NY 14260, USA.

^h Synchrotron SOLEIL, L'Orme des Merisiers, St. Aubin, BP 48, 91192 Gif sur Yvette, France.

Email: laurent.nahon@synchrotron-soleil.fr.

A. Calculated UV/vis absorption and ECD spectra: computational details and comparison with experiment

The UV/vis absorption and ECD spectra were calculated for the Λ -Ru(acac)₃ stereoisomer via TDDFT linear response calculations of the energies and associated dipole and rotatory strength values for the 150 lowest allowed singly excited states. To match experimental measurements conditions, the computations were performed with inclusion of solvent effects to model dichloromethane (CH₂Cl₂, $\epsilon = 8.9$) solution.

The geometry of the Λ -Ru(acac)₃ complex was optimized with DFT using the Turbomole program, version 6.5 (TM6.5),^{1,2,3} imposing C_2 symmetry and employing the global hybrid B3LYP^{4,5,6} density functional as implemented in TM6.5. The TZVP basis set⁷ was used for all atoms along with the corresponding 28-electron scalar relativistic effective core potential (ECP) for Ru.⁸ The solvent effects were treated in the calculations via the conductor-like screening model (COSMO)^{9,10} with default parameters.

The TDDFT linear response calculations employed the TZVP-ECP basis set and two density functionals: (i) B3LYP that has recently been successfully used in the quantum-

chemical description of experimentally observed spectral features and their modifications upon one-electron redox processes for ruthenium(III)-tris(β -diketonato) complexes with ligands containing an elongated alkyl substituent (butyl, octyl) in the 3 position of the acetylacetone ion;¹¹ and (ii) optimally tuned range-separated hybrid LC-PBE0* (25% of exact exchange in the short-range limit of interelectronic distances; an error function range-separation parameter γ^* of 0.1 (bohr)⁻¹),^{12,13,14,15} the parametrization of which is expected to mitigate the electron delocalization error^{16,17} and reproduce the photoemission characteristics well from the orbital energy spectrum.^{15,18,19} Note that all our attempts to obtain the corresponding TDDFT-simulated spectra with the LB94²⁰ potential failed due to problems with reaching Self-Consistent Field (SCF) convergence for the ground state of unrestricted C_2 -symmetric $A\text{-Ru(acac)}_3$ structure. The computations employing LC functional parametrizations were carried out using the Gaussian 09 program, revision D.01 (G09);²¹ otherwise TM6.5 was utilized. Solvent effects (CH_2Cl_2) in the linear response calculations were treated via COSMO²² and the polarizable continuum model (PCM)^{9,23} in the case of TM6.5 and G09, respectively. As for open-shell systems full TDDFT tends to have ground-state (near) instability problems,^{24,25} validity of the TDDFT results was supported by performing analogous UV/vis absorption and ECD calculations with the Tamm-Danoff approximation (TDA).^{26,27,28} The TDDFT-TDA calculations gave essentially the same spectra in the considered energy spectral range, as shown in Fig. S3. The calculated spectra presented here were obtained as the sums of Gaussian functions centered at the vertical excitation energies and scaled according to the calculated oscillator or rotatory strengths, with a root mean square width parameter of 0.2 eV.²⁹ Fig. S3 also displays the experimental ECD spectrum.

The experimental and simulated UV/visible absorption and ECD spectra based on TDDFT calculations with a continuum solvent model for CH_2Cl_2 are presented in Fig. S4; see panels a-b (experimental) and c-d (calculated). As can be seen in both Fig. S3 and Fig. S4, despite providing better ionization characteristics of Ru(acac)_3 (see Table 1 in the main text), LC-PBE0* does not outperform B3LYP in reproducing the experimental UV/visible absorption and ECD spectra for the complex. Namely, although with both functionals very similar spectral envelopes (reproducing well the experiments) were obtained, the spectra modelled with LC-PBE0* demonstrate a pronounced blue shift reflecting the increase in the orbital energy gap observed for this functional as compared to B3LYP and deteriorating the agreement between computed and experimental data. Accordingly, the assignment of the spectra presented below was based on an analysis of the B3LYP results.

Dominant excitations responsible for the observed UV/visible absorption and ECD spectral features as computed with B3LYP for Λ -Ru(acac)₃ are shown in Fig. S5 and listed in Table S2 along with their underlying MO-to-MO electronic transitions. The corresponding MOs isosurfaces are presented in Fig. S6 and S7. The MO-pairs analysis of the intense excitations of Λ -Ru(acac)₃ revealed that the main positive band observed in its ECD spectrum around 350 nm originates from excitations that are assigned as predominantly metal-to-ligand (ML) charge transfers (CTs) within α -spin MO sets, from the nonbonding Ru d _{π} to the acac-centered π^* -orbitals (see excitations no. 26, 27, 30 computed at 335, 332 and 324 nm, respectively). The broad negative intensity between around 375-500 nm is due to several intense excitations demonstrating both negative and positive rotatory strength values with a clear dominance of the former and revealing generally a mixed ML and ligand-to-metal (LM) CT character with some contributions from metal-to-metal (MM) transitions. For example, excitation no. 4 (468 nm) corresponds mainly to π - π^* LM CT from the β -occupied metal-ligand bonding MO to the lowest-energy unoccupied MO representing an “electron hole” in the β -spin density, excitations nos. 9 (411 nm) and 23 (354 nm) can be assigned as predominantly ML CTs, while excitation no. 20 (364 nm) involves MM transitions from the nonbonding Ru d _{π} orbitals to the metal-centered antibonding MOs of local σ symmetry with respect to the Ru–O bonds. Finally, the lowest-energy band, of modest positive intensity, which appears in the experimental ECD spectrum of Λ -Ru(acac)₃ around 550 nm, results from π - π^* LM CT involving the β -occupied acac MO and the d _{π} β “electron hole” (see excitation no. 3, 485 nm). The presented assignments of dominant excitations are in line with those reported in References 11 and 30; the nature of such excitations is also qualitatively the same in the LC-PBE0* calculations (see Fig. S8-S10 and Table S3).

B. Additional figures

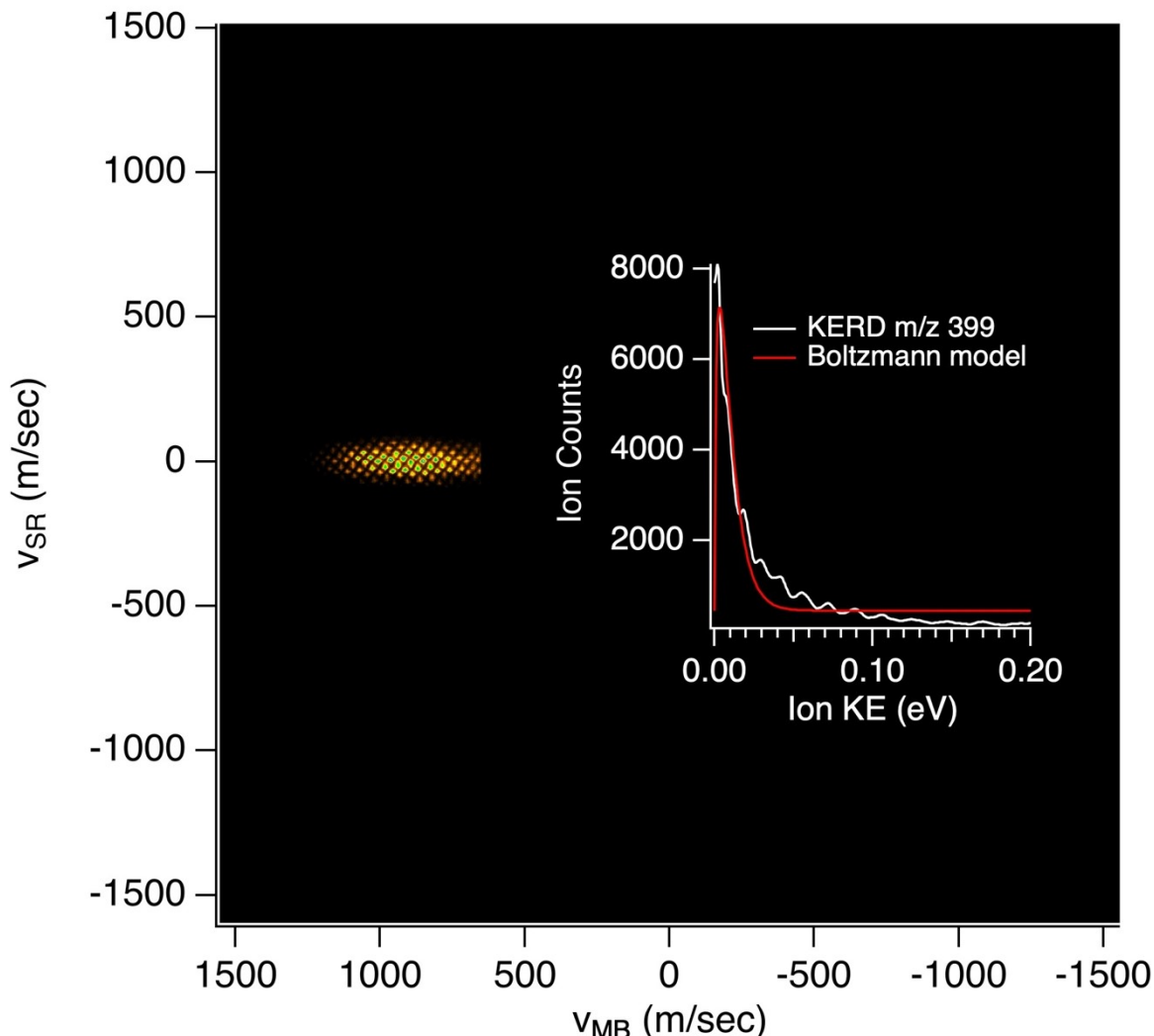


Fig. S1. Mass selected ion velocity image for the parent $\text{Ru}(\text{acac})_3$ (m/z 399) ion recorded at a photon energy of 8 eV in 3D momentum imaging mode, *i.e.* applying electrostatic lenses to the second acceleration region of the Wiley-McLaren spectrometer.³¹ The bottom axis corresponds to the molecular beam (MB) propagation direction (from right to left), while the vertical axis represents the synchrotron radiation (SR) direction. The corresponding ion kinetic energy release distribution (KERD) in eV is shown in the inset, along with a Boltzmann model from which a translational temperature of 80 K is deduced.

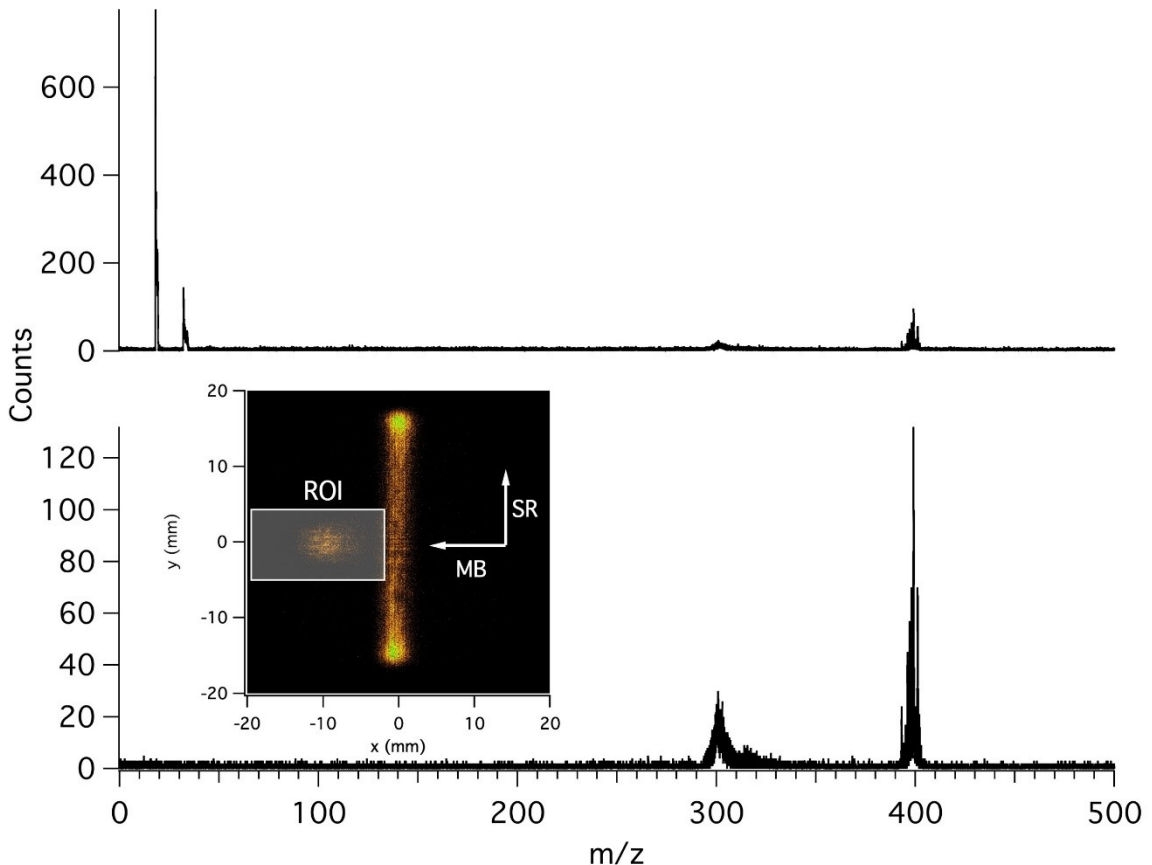


Fig. S2. (a) Raw mass spectrum of $\text{Ru}(\text{acac})_3$ recorded at 14 eV; (b) ROI-filtered mass spectrum where only ions that fall within the region of interest (ROI) defined in the inset are taken into account. The effect of the filtering is to remove the thermal contribution from water and oxygen present in the chamber as background, but not in the cold molecular beam. The background gas leads to a much elongated interaction region along the synchrotron radiation (SR) direction, but no net velocity along the molecular beam (MB) direction, while the molecules coming out of the oven's nozzle exhibit the opposite behavior due to the MB velocity and spatial collimation.

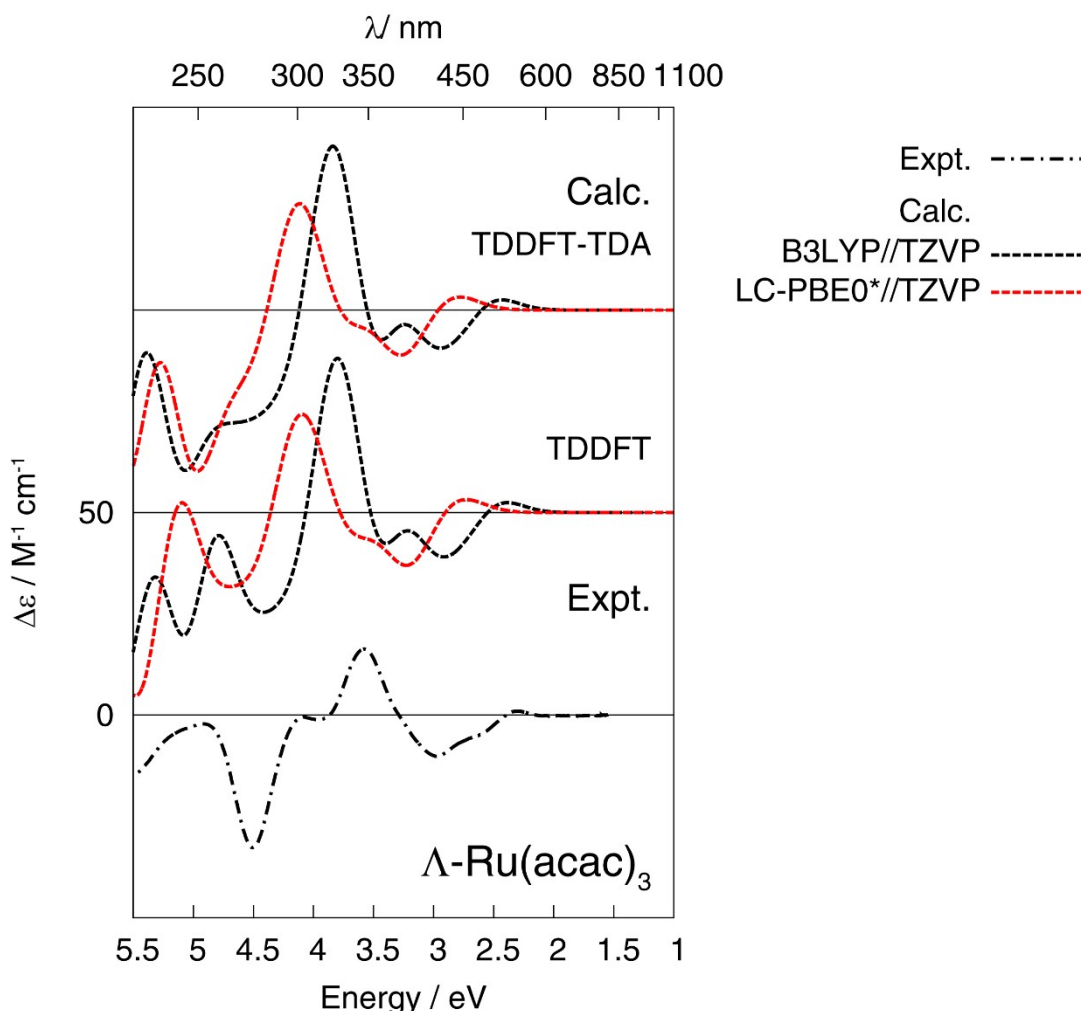


Fig. S3. Comparison of the experimental and calculated ECD spectra of $\Lambda\text{-Ru}(\text{acac})_3$. No spectral shift has been applied. Full TDDFT (TDDFT) and TDDFT with Tamm-Danoff approximation (TDDFT-TDA) calculations with the B3LYP and LC-PBE0* density functionals, TZVP basis set, and with inclusion of solvent (dichloromethane) effects.

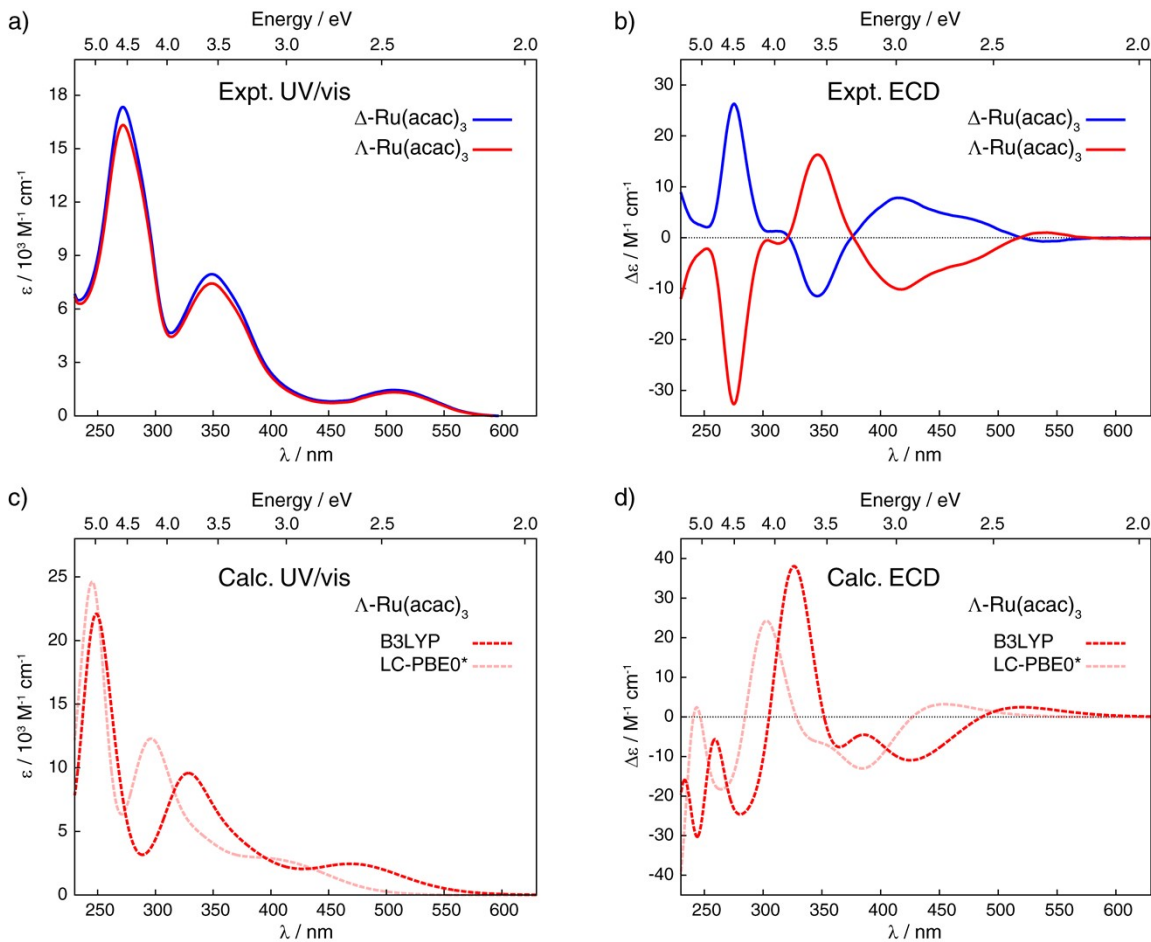


Fig. S4. Experimental UV/vis absorption (panel a) and ECD (panel b) spectra of Δ and Λ enantiomers of Ru(acac)₃ recorded in dichloromethane (at concentrations of 5×10^{-4} M) along with the corresponding TDDFT-simulated (calculations with the B3LYP and LC-PBE0* density functionals, TZVP basis set, and with inclusion of solvent – dichloromethane – effects) spectra for Λ -Ru(acac)₃ (panel c and d for UV/vis absorption and ECD spectra, respectively).

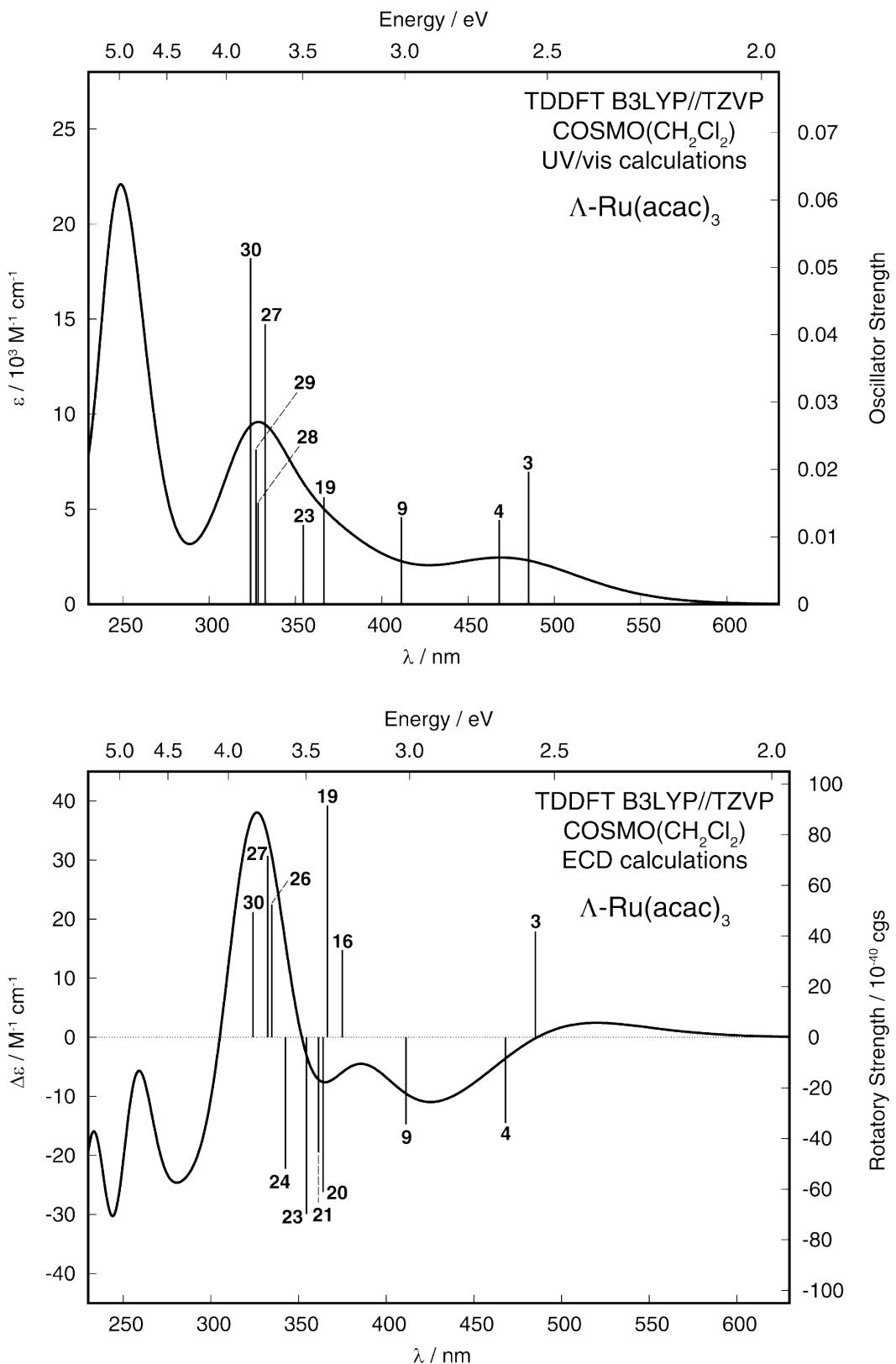


Fig. S5. Simulated (TDDFT B3LYP//TZVP calculations with continuum solvent model for dichloromethane) UV/vis absorption (top) and ECD (bottom) spectra of $\Lambda\text{-Ru}(\text{acac})_3$. No spectral shift has been applied. Calculated excitation energies and oscillator / rotatory strengths indicated as ‘stick’ spectra. Numbered excitations correspond to those analyzed in detail in Table S2.

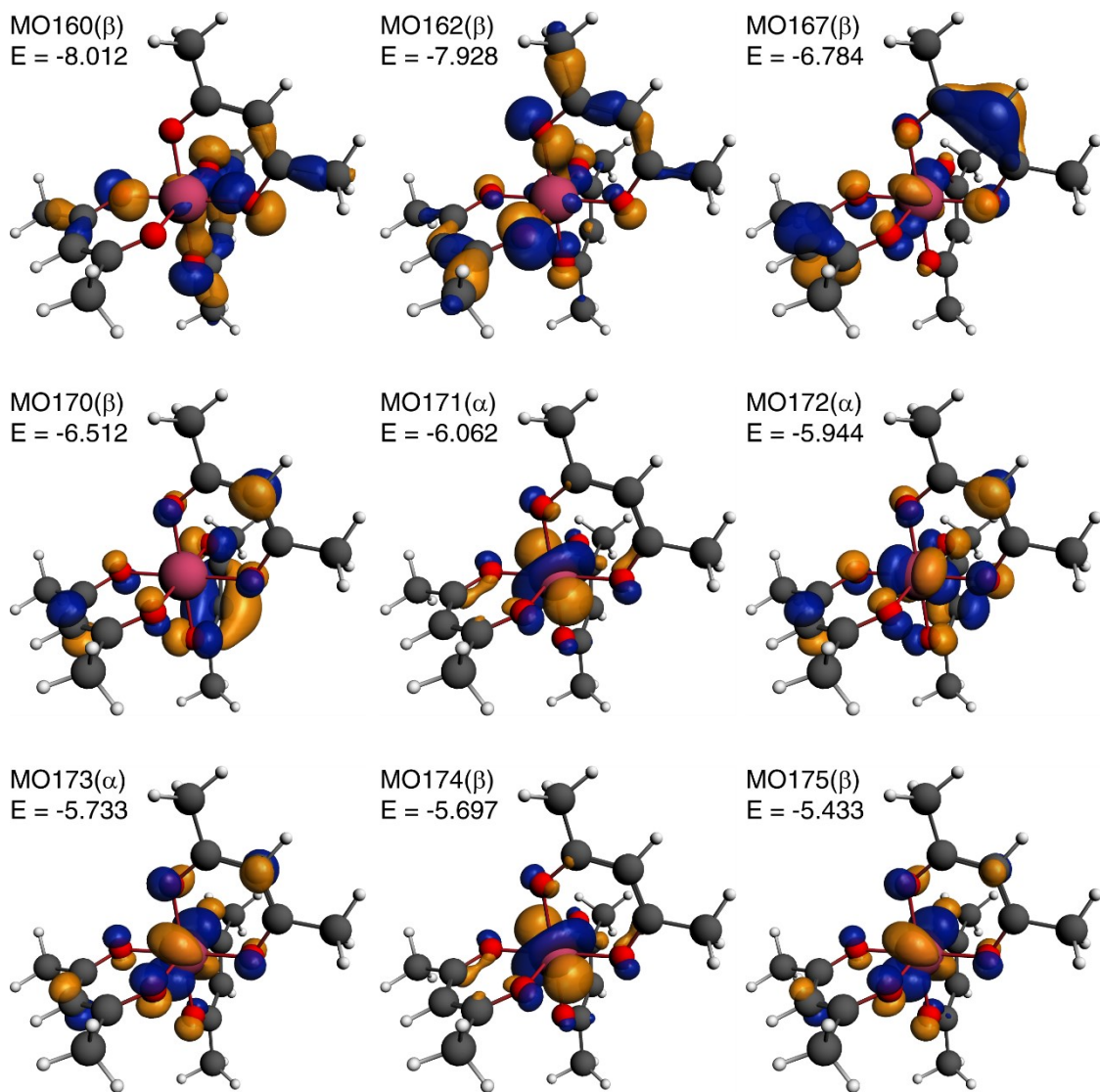


Fig. S6. Isosurfaces ($\pm 0.05 \sqrt{e^-/(bohr)^3}$) of α -spin and β -spin occupied molecular orbitals involved in selected B3LYP-computed transitions of $\Lambda\text{-Ru}(\text{acac})_3$. B3LYP//TZVP calculations with continuum solvent model for dichloromethane. E = orbital energy, in eV. Note that in Fig. S13 MOs obtained from the gas-phase calculations are presented.

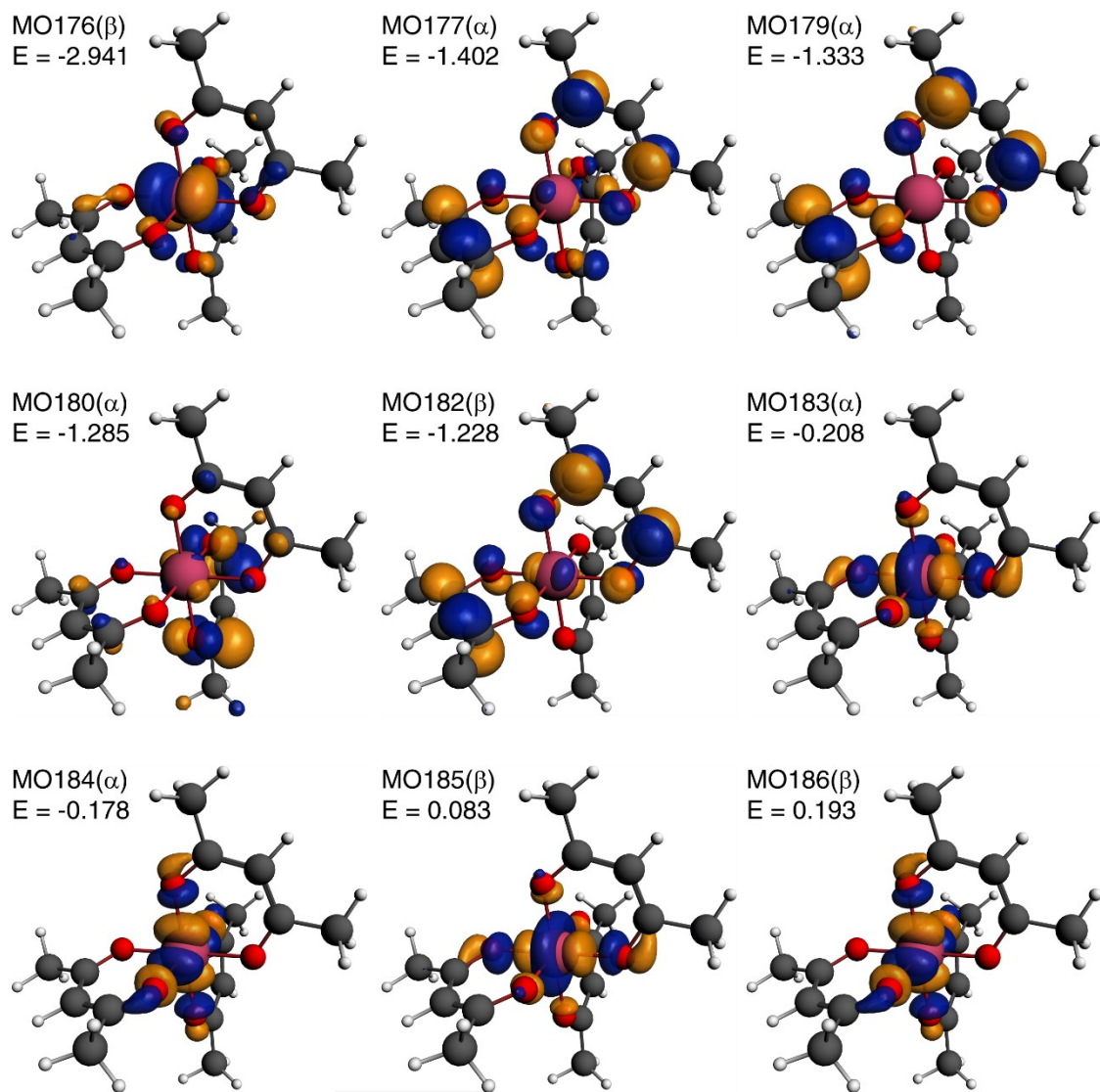


Fig. S7. Isosurfaces ($\pm 0.05 \sqrt{e^-/(bohr)^3}$) of α -spin and β -spin unoccupied molecular orbitals involved in selected B3LYP-computed transitions of $\Lambda\text{-Ru}(\text{acac})_3$. B3LYP//TZVP calculations with continuum solvent model for dichloromethane. E = orbital energy, in eV. Note that in Fig. S13 MOs obtained from the gas-phase calculations are presented.

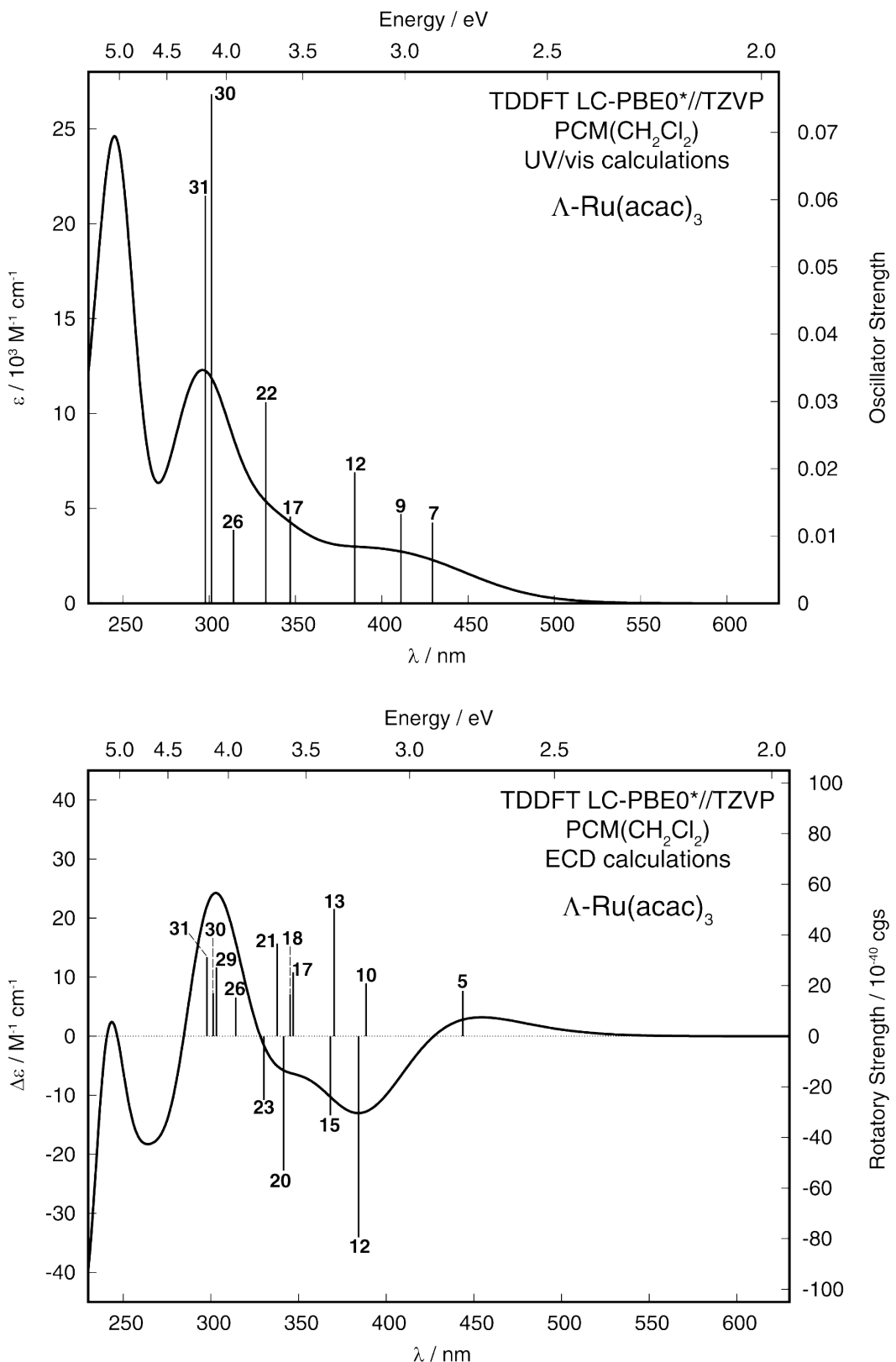


Fig. S8. Simulated (TDDFT LC-PBE0*/TZVP calculations with continuum solvent model for dichloromethane) UV/vis absorption (top) and ECD (bottom) spectra of $\Lambda\text{-Ru}(\text{acac})_3$. No spectral shift has been applied. Calculated excitation energies and oscillator / rotatory strengths indicated as ‘stick’ spectra. Numbered excitations correspond to those analyzed in detail in Table S3.

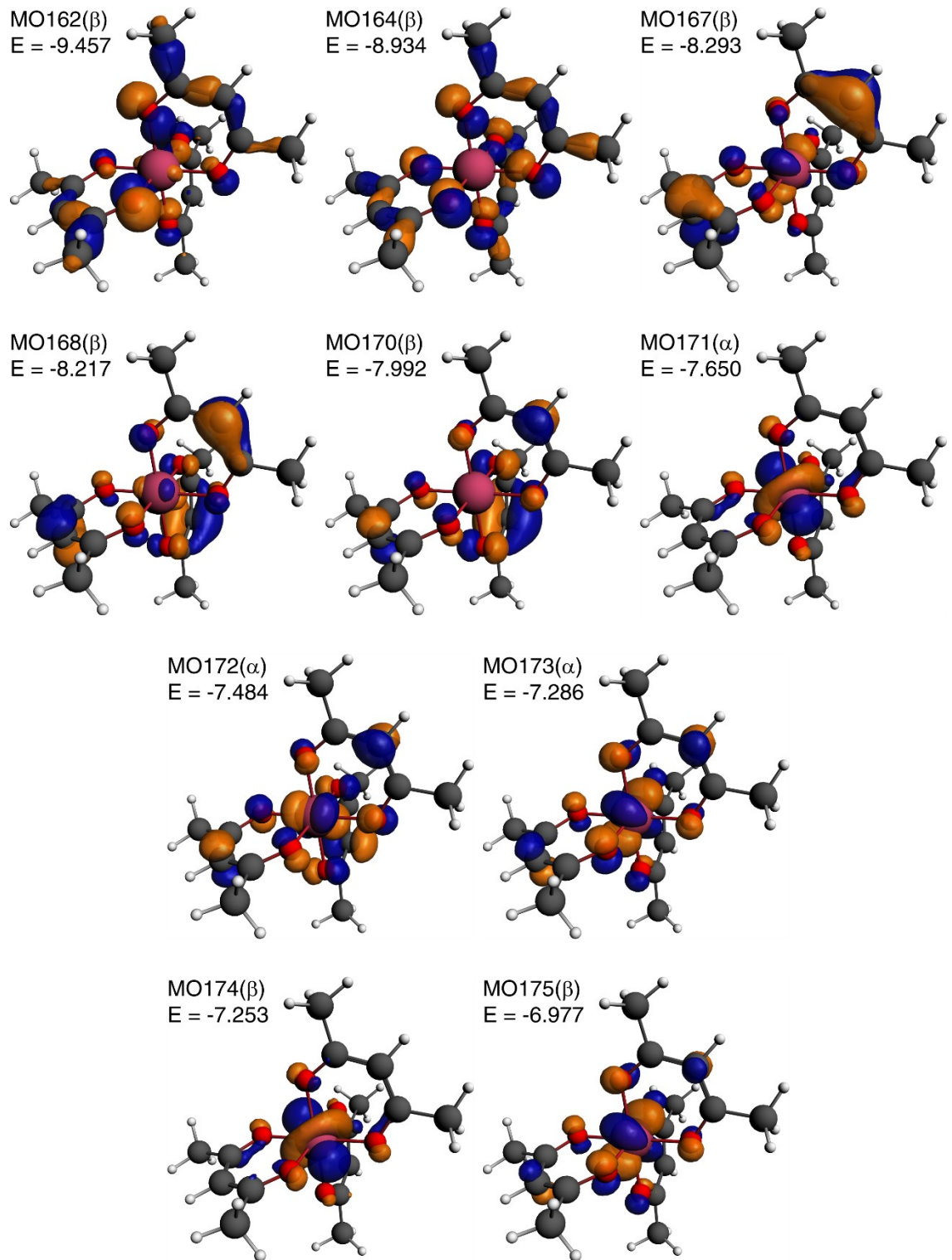


Fig. S9. Isosurfaces ($\pm 0.05 \sqrt{e^-/(bohr)^3}$) of α -spin and β -spin occupied molecular orbitals involved in selected LC-PBE0*-computed transitions of $\Lambda\text{-Ru}(\text{acac})_3$. LC-PBE0*//TZVP calculations with continuum solvent model for dichloromethane. E = orbital energy, in eV. Note that in Fig. S12 MOs obtained from the gas-phase calculations are presented.

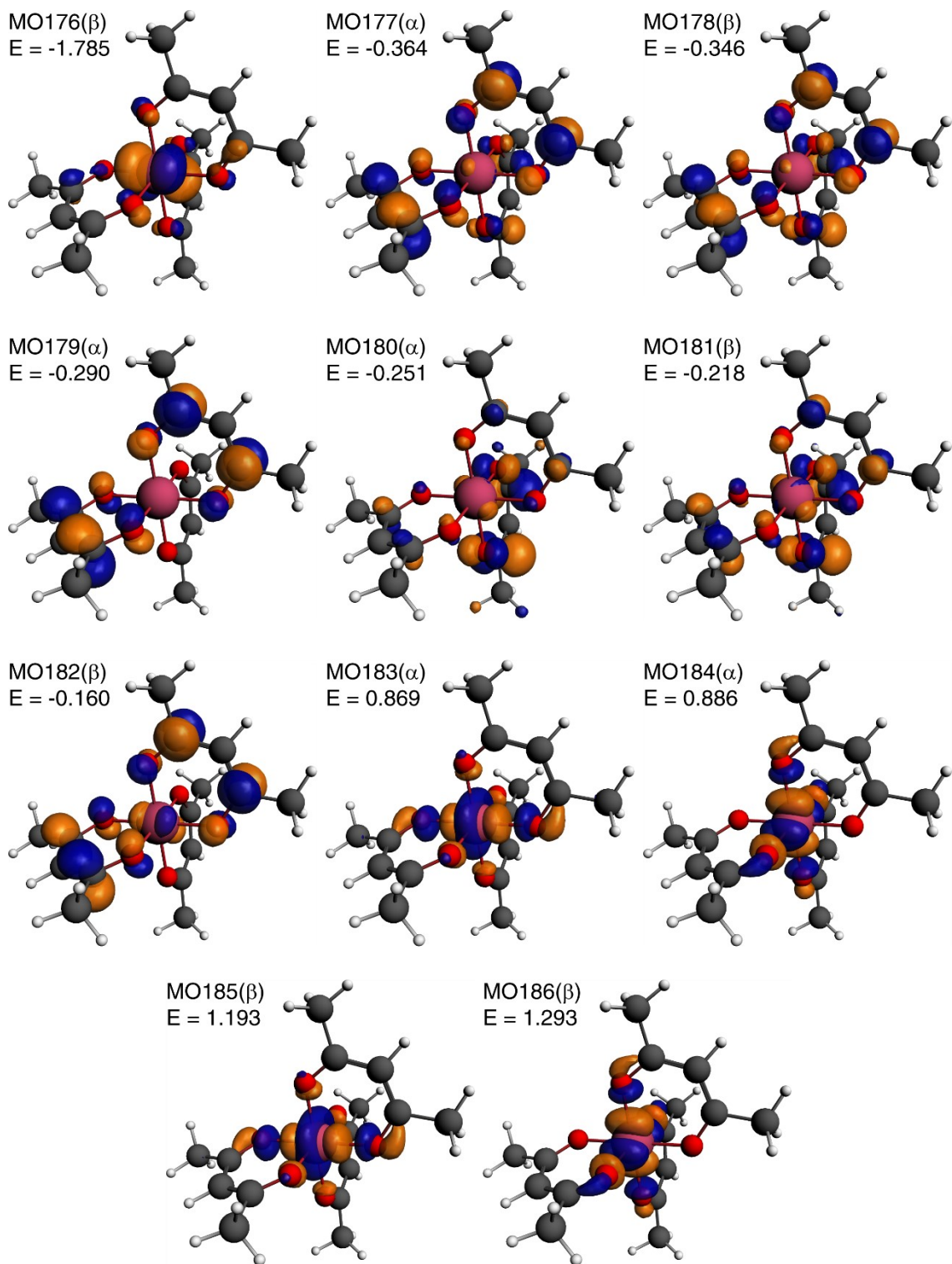


Fig. S10. Isosurfaces ($\pm 0.05 \sqrt{e^-/(bohr)^3}$) of α -spin and β -spin unoccupied molecular orbitals involved in selected LC-PBE0*-computed transitions of Λ -Ru(acac)₃. LC-PBE0*/TZVP calculations with continuum solvent model for dichloromethane. E = orbital energy, in eV. Note that in Fig. S12 MOs obtained from the gas-phase calculations are presented.

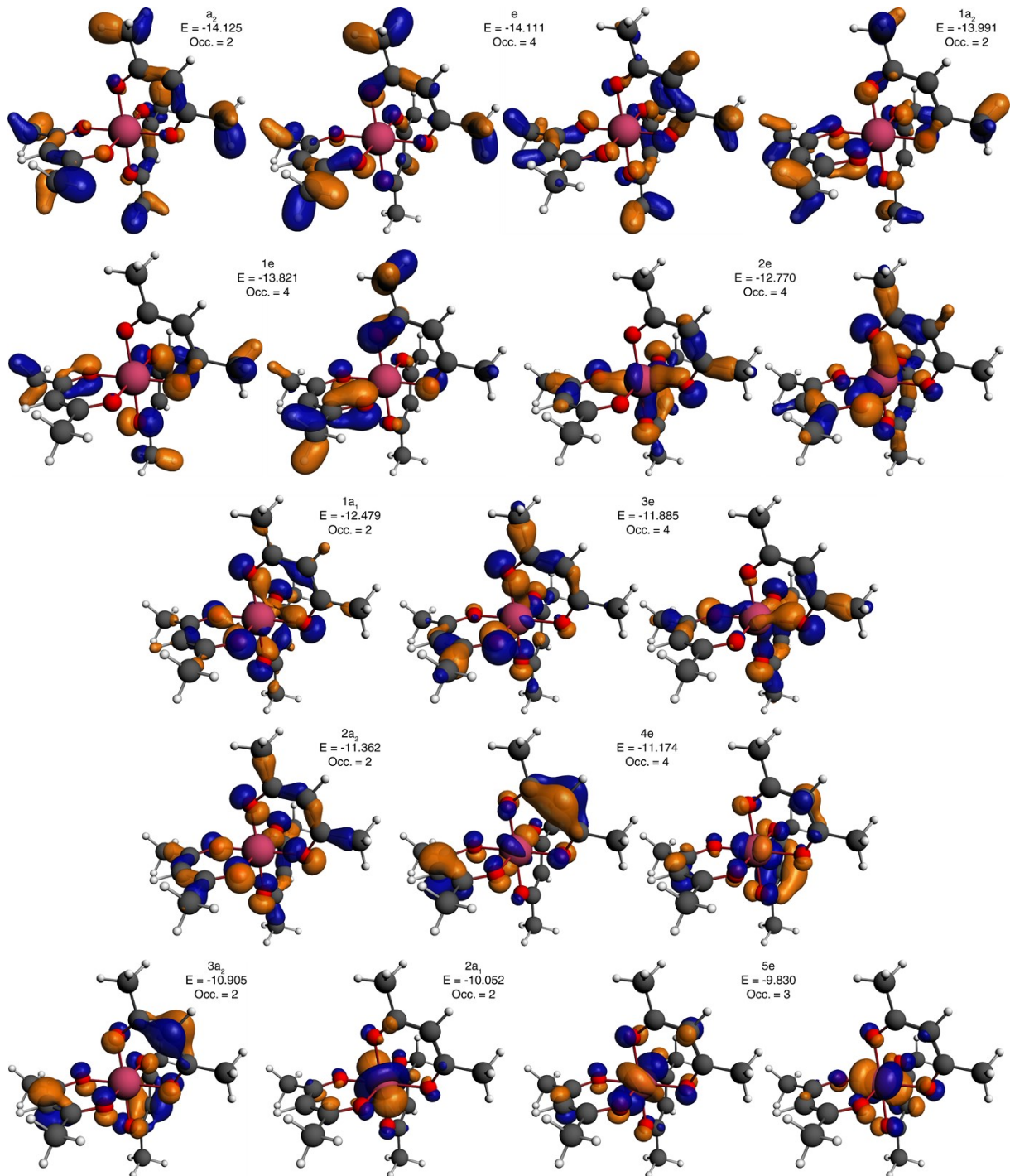


Fig. S11. Isosurfaces ($\pm 0.05 \sqrt{e^-/(bohr)^3}$) of the outermost molecular orbitals calculated using LB94//TZP/DZP (gas-phase) at VWN-optimized D_3 -symmetry structure of $A\text{-Ru}(\text{acac})_3$ in its closed-shell configuration. #irreducible-representation (molecular orbital number and its symmetry, listed in order of increasing energy). E = orbital energy, in eV. Occ. = occupation. The corresponding MOs obtained with LB94//B-spline are expected to be very similar and therefore they are not shown.

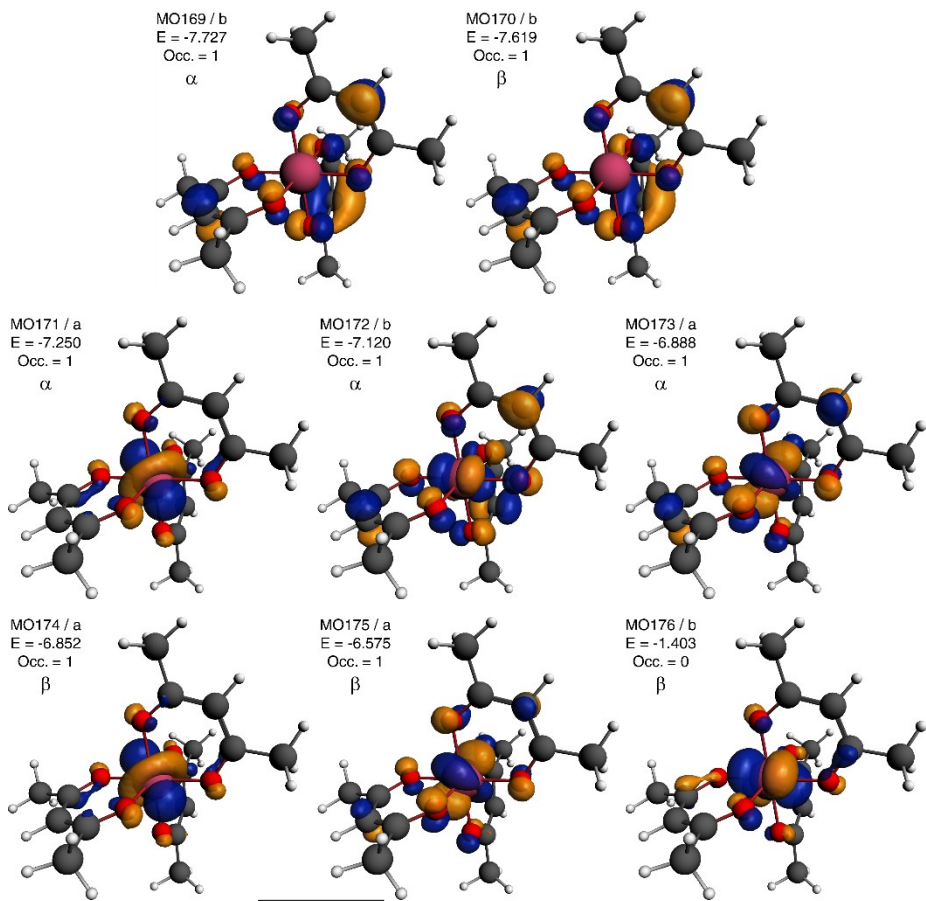


Fig. S12. Isosurfaces ($\pm 0.05 \sqrt{e^-/(bohr)^3}$) of the frontier α -spin and β -spin molecular orbitals calculated using LC-PBE0*//TZVP (gas-phase) at B3LYP-optimized C_2 -symmetry structure of Λ -Ru(acac)₃; compare with MOs 5e, 2a₁ and 3a₂ presented in Fig. S11 and MOs presented in Fig. S13. MO# (molecular orbital number listed in order of increasing energy) / orbital symmetry. E = orbital energy, in eV. Occ. = occupation.

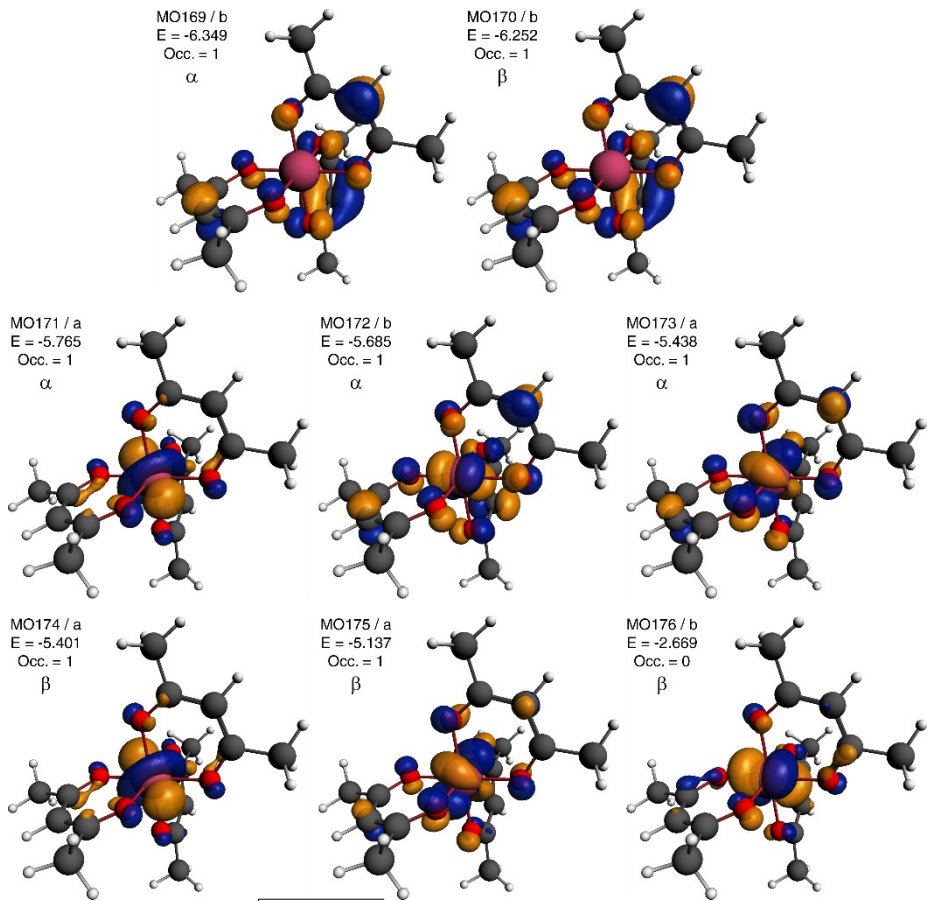


Fig. S13. Isosurfaces ($\pm 0.05 \sqrt{e^-/(bohr)^3}$) of the frontier α -spin and β -spin molecular orbitals calculated using B3LYP//TZVP (gas-phase) at B3LYP-optimized C_2 -symmetry structure of $A\text{-Ru}(\text{acac})_3$; compare with MOs 5e, 2a₁ and 3a₂ presented in Fig. S11 and MOs presented in Fig. S12. MO# (molecular orbital number listed in order of increasing energy) / orbital symmetry. E = orbital energy, in eV. Occ. = occupation.

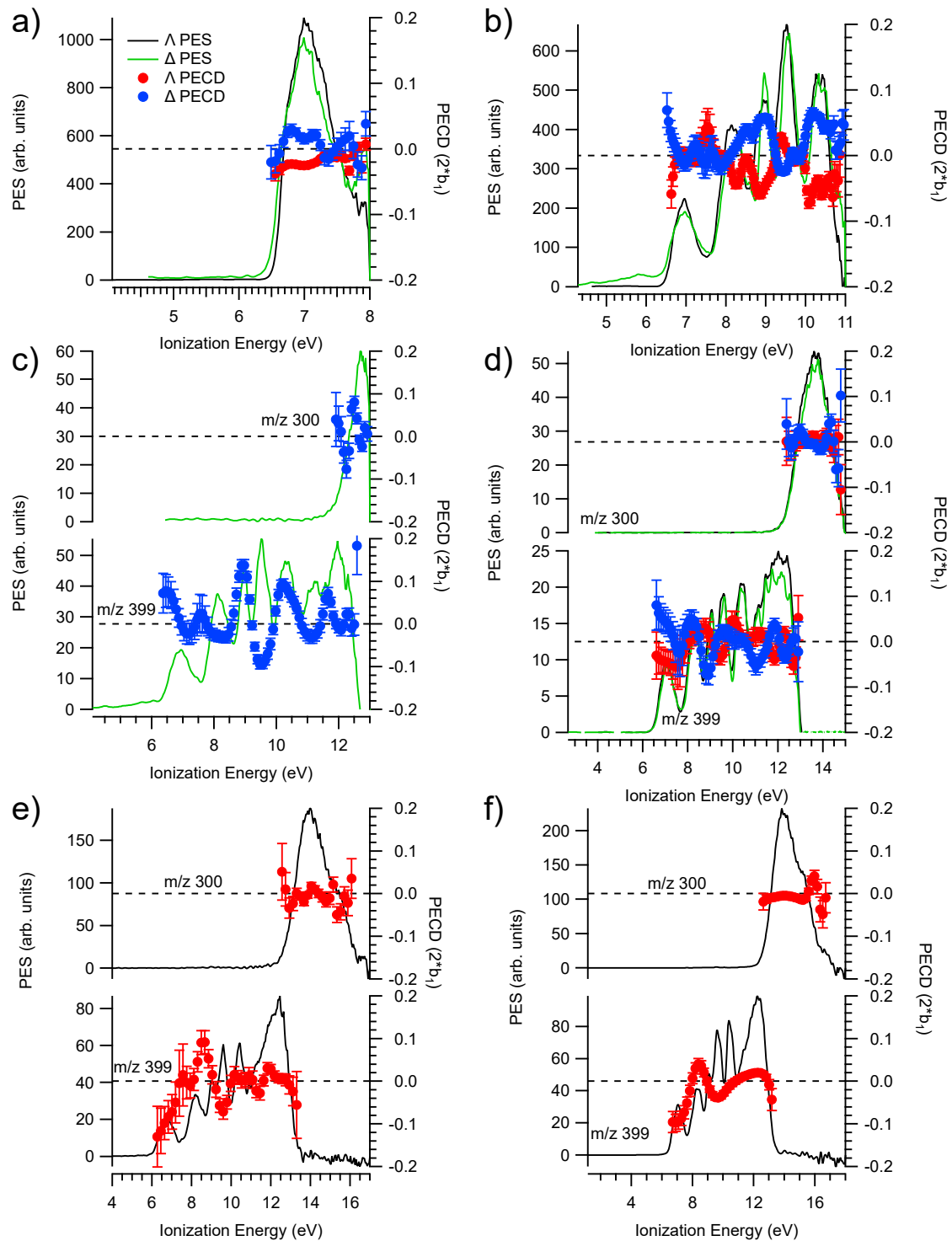


Fig. S14. PECD and PES curves of the parent $\text{Ru}(\text{acac})_3$ ion (m/z 399) and its fragment $\text{Ru}(\text{acac})_2$ ion from dissociative ionization (m/z 300), recorded at photon energies of 8 eV (a), 11 eV (b), 13 eV (c), 15 eV (d), 17 eV (e) and 18 eV (f).

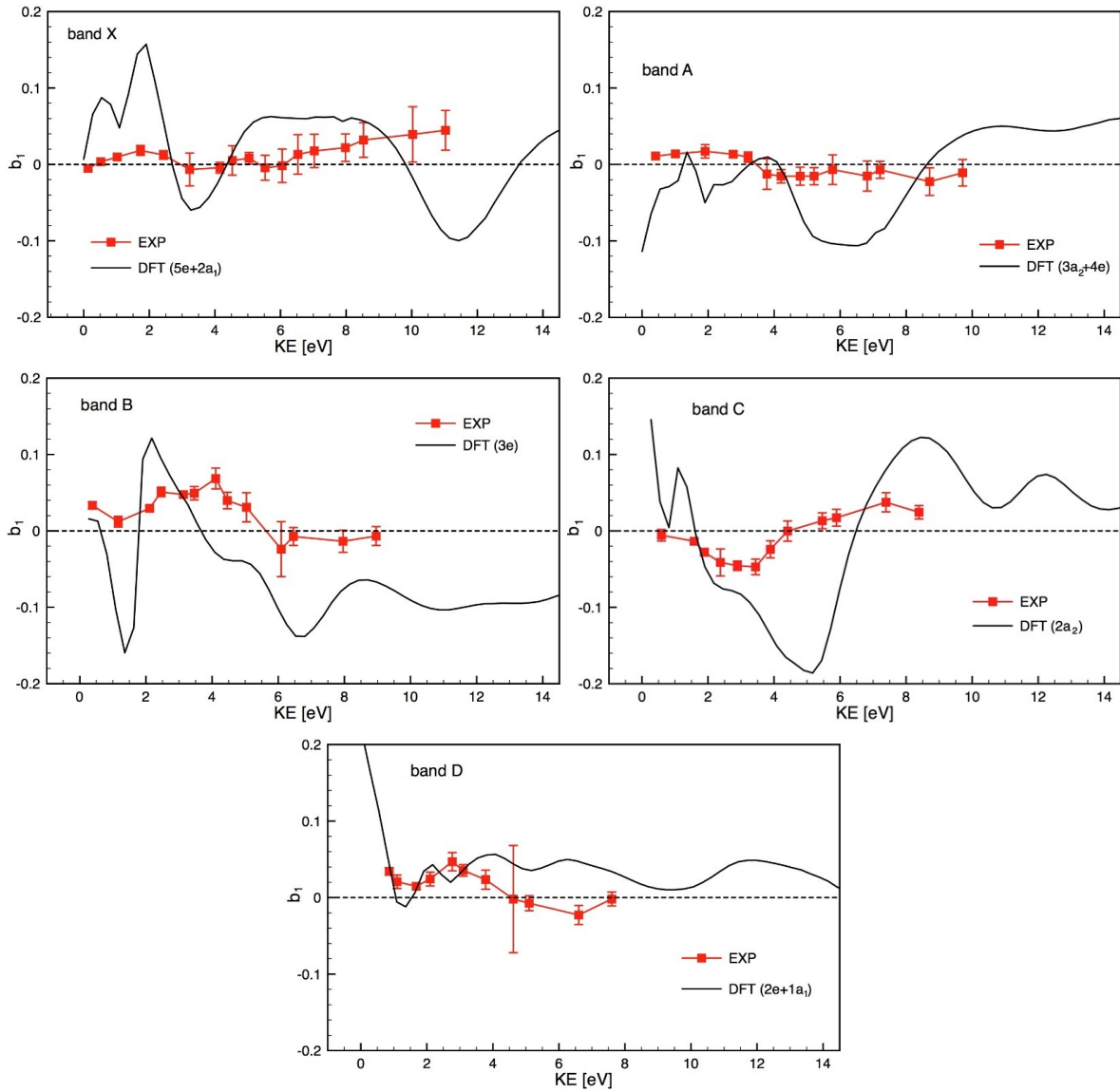


Fig. S15. Comparison of the experimental PECD data (EXP) and calculated DFT profiles of the dichroic parameter b_1 versus electron kinetic energy for the bands X to D identified in the PES (see Figs. 3 and 4) and listed in Table 2 (the experimental data are already shown in Fig. 5). Due to the composite nature of the experimental bands (see Table 2) each calculated profile is an average over the contributing ionization channels, weighted by the corresponding calculated cross sections.

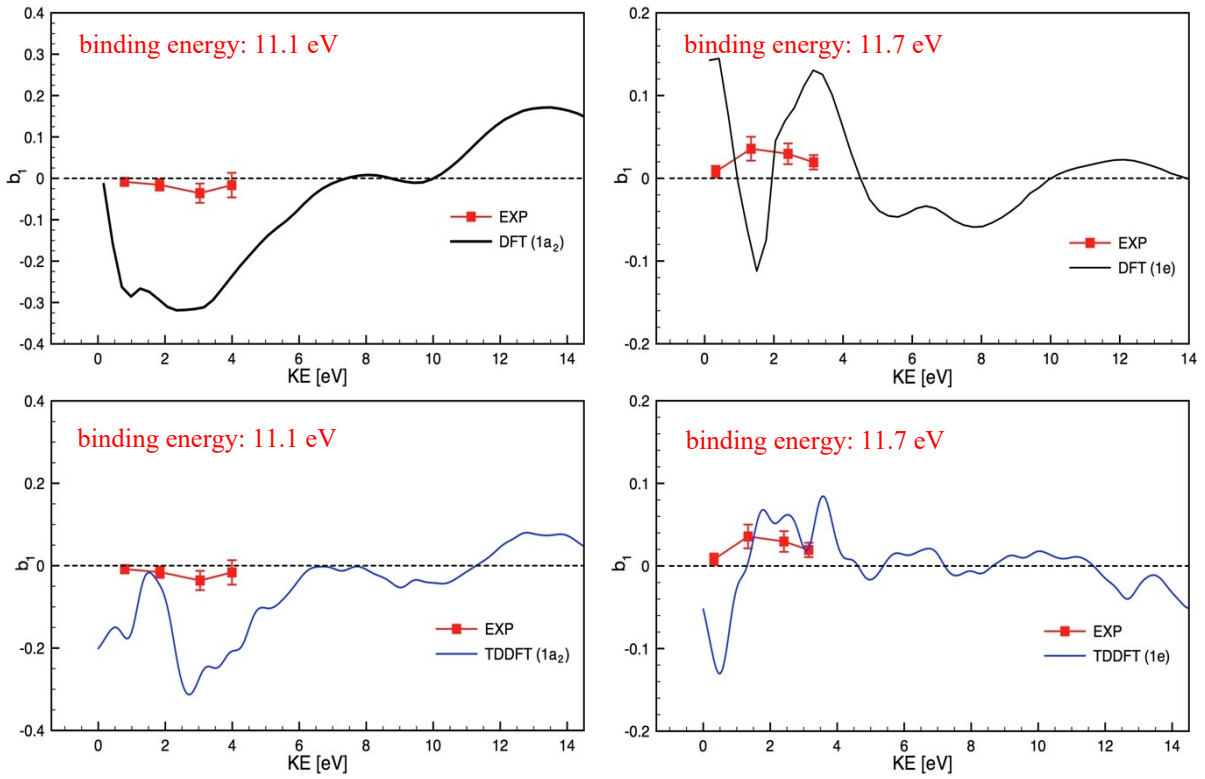


Fig. S16. Comparison of the experimental PECD data (EXP) and calculated DFT and TDDFT profiles of the dichroic parameter b_1 versus electron kinetic energy at binding energies of 11.1 eV and 11.7 eV, within the composite band E identified in the PES (see Figs. 3 and 4, and Table 2).

C. Additional tables

Table S1. Values of the target functional J (see definition below) as a function of the range-separation parameter γ calculated with LC-PBE0 for Ru(acac)₃. Optimal value of the range-separation parameter, defining optimally tuned parametrization LC-PBE0*, is highlighted in bold.

$\gamma / (\text{bohr})^{-1}$	J / eV^a
0.05	0.53603
0.10	0.04037
0.15	0.36654
0.20	0.68894
0.22	0.79780
0.25	0.94227
0.27	1.02749
0.30	1.14082
0.35	1.29779
0.40	1.42273
0.45	1.52349
0.50	1.60481

$$^a J = |\epsilon^{\text{HOMO}}(\text{Ru(acac)}_3) + \text{IE}^{\text{vert}}(\text{Ru(acac)}_3)| = |\epsilon^{\text{HOMO}}(\text{Ru(acac)}_3) + E_{\text{gs}}([\text{Ru(acac)}_3]^+) - E_{\text{gs}}(\text{Ru(acac)}_3)|$$

where:

$\epsilon^{\text{HOMO}}(\text{Ru(acac)}_3)$ – energy of the highest occupied molecular orbital (HOMO) in the neutral system, Ru(acac)₃, with a doublet spin electronic configuration

$E_{\text{gs}}([\text{Ru(acac)}_3]^+)$ – ground-state energy of the cationic system, [Ru(acac)₃]⁺, with a triplet spin electronic configuration

$E_{\text{gs}}(\text{Ru(acac)}_3)$ – ground-state energy of the neutral system, Ru(acac)₃, with a doublet spin electronic configuration

Table S2. Selected dominant B3LYP-computed excitations and occupied (occ) – unoccupied (unocc) molecular orbital pair contributions (greater than 10%) of $\text{A-Ru}(\text{acac})_3$. For simulated spectra, see Figs. S4 and S5; for molecular orbitals isosurfaces, see Figs. S6 and S7.

Excitation	E / eV	λ / nm	f	R / 10^{-40} cgs	occ no.	unocc no.	%	Dominant assignment ^a
#3	2.56	485	0.0197	41.80	170(β)	176(β)	76.5	$\text{L}\pi \rightarrow \text{M}\pi$
#4	2.65	468	0.0125	-34.00	167(β)	176(β)	70.7	$\text{M-L}\pi \rightarrow \text{M}\pi$
					175(β)	182(β)	11.0	$\text{M(-L)}\pi \rightarrow (\text{M-})\text{L}\pi$
#9	3.01	411	0.0129	-34.44	175(β)	182(β)	34.3	$\text{M(-L)}\pi \rightarrow (\text{M-})\text{L}\pi$
					173(α)	179(α)	17.7	$\text{M(-L)}\pi \rightarrow \text{L}\pi$
					167(β)	176(β)	17.6	$\text{M-L}\pi \rightarrow \text{M}\pi$
#16	3.31	375	0.0079	34.46	175(β)	182(β)	30.0	$\text{M(-L)}\pi \rightarrow (\text{M-})\text{L}\pi$
					173(α)	179(α)	23.2	$\text{M(-L)}\pi \rightarrow \text{L}\pi$
#19	3.38	366	0.0159	91.61	174(β)	182(β)	65.9	$\text{M}\pi \rightarrow (\text{M-})\text{L}\pi$
#20	3.41	364	0.0033	-61.14	175(β)	186(β)	26.1	$\text{M(-L)}\pi \rightarrow \text{M}\sigma$
					173(α)	184(α)	19.4	$\text{M(-L)}\pi \rightarrow \text{M}\sigma$
					172(α)	177(α)	17.6	$\text{M(-L)}\pi \rightarrow (\text{M-})\text{L}\pi$
#21	3.43	361	0.0081	-45.62	173(α)	180(α)	65.9	$\text{M(-L)}\pi \rightarrow (\text{M-})\text{L}\pi$
					173(α)	177(α)	11.0	$\text{M(-L)}\pi \rightarrow (\text{M-})\text{L}\pi$
#23	3.50	354	0.0118	-69.84	173(α)	179(α)	24.9	$\text{M(-L)}\pi \rightarrow \text{L}\pi$
					172(α)	183(α)	12.0	$\text{M(-L)}\pi \rightarrow \text{M}\sigma$
					172(α)	177(α)	10.4	$\text{M(-L)}\pi \rightarrow (\text{M-})\text{L}\pi$
#24	3.62	343	0.0072	-52.02	172(α)	179(α)	30.5	$\text{M(-L)}\pi \rightarrow \text{L}\pi$
					173(α)	177(α)	21.0	$\text{M(-L)}\pi \rightarrow (\text{M-})\text{L}\pi$
#26	3.70	335	0.0073	52.44	171(α)	177(α)	35.4	$\text{M}\pi \rightarrow (\text{M-})\text{L}\pi$
					173(α)	183(α)	14.7	$\text{M(-L)}\pi \rightarrow \text{M}\sigma$
					175(β)	185(β)	14.6	$\text{M(-L)}\pi \rightarrow \text{M}\sigma$
					160(β)	176(β)	11.4	$(\text{M-})\text{L}\sigma \rightarrow \text{M}\pi$

#27	3.73	332	0.0415	71.69	171(α) 162(β)	179(α) 176(β)	44.3 13.7	Mπ → Lπ (M-)Lσ → Mπ
#28	3.78	328	0.015	21.83	162(β) 171(α)	176(β) 179(α)	53.6 30.9	(M-)Lσ → Mπ Mπ → Lπ
#29	3.79	327	0.023	9.28	160(β) 171(α)	176(β) 177(α)	55.2 12.2	(M-)Lσ → Mπ Mπ → (M-)Lπ
#30	3.83	324	0.0514	49.48	171(α) 172(α) 171(α)	180(α) 184(α) 177(α)	30.4 13.6 11.9	Mπ → (M-)Lπ M(-L)π → Mσ Mπ → (M-)Lπ

^a Mπ = metal-centered π MO (metal-based *d*π orbital)

Mσ = metal-centered σ MO (metal-based *d*σ orbital)

Lπ = ligand-centered π MO

M-Lπ = metal-ligand-centered π MO

(M-)Lπ = ligand-centered π MO with non-negligible metal *d*π orbital involvement

M(-L)π = metal-centered π MO with non-negligible ligand π orbitals involvement

(M-)Lσ = ligand-centered σ MO with non-negligible metal *d*σ orbital involvement

Table S3. Selected dominant LC-PBE0*-computed excitations and occupied (occ) – unoccupied (unocc) molecular orbital pair contributions (greater than 10%) of Λ -Ru(acac)₃. For simulated spectra, see Figs. S4 and S8; for molecular orbitals isosurfaces, see Figs. S9 and S10.

Excitation	E / eV	λ / nm	f	R / 10^{-40} cgs	occ no.	unocc no.	%	Dominant assignment ^a
5	2.79	444	0.005	17.93	170(β)	176(β)	23.6	$L\pi \rightarrow M\pi$
					174(β)	185(β)	20.0	$M\pi \rightarrow M\sigma$
					171(α)	183(α)	14.8	$M\pi \rightarrow M\sigma$
7	2.89	429	0.012	12.63	170(β)	176(β)	37.4	$L\pi \rightarrow M\pi$
					174(β)	185(β)	18.4	$M\pi \rightarrow M\sigma$
					171(α)	183(α)	13.8	$M\pi \rightarrow M\sigma$
9	3.02	411	0.013	1.07	168(β)	176(β)	38.3	(M-)L $\pi \rightarrow M\pi$
					170(β)	176(β)	28.6	$L\pi \rightarrow M\pi$
10	3.19	388	0.004	20.93	168(β)	176(β)	39.2	(M-)L $\pi \rightarrow M\pi$
					173(α)	177(α)	11.5	$M(-L)\pi \rightarrow (M-L)\pi$
12	3.23	384	0.020	-79.49	167(β)	176(β)	42.5	$M-L\pi \rightarrow M\pi$
					173(α)	179(α)	13.2	$M(-L)\pi \rightarrow L\pi$
13	3.35	370	0.003	50.30	173(α)	184(α)	38.7	$M(-L)\pi \rightarrow M\sigma$
					175(β)	186(β)	37.4	$M(-L)\pi \rightarrow M\sigma$
15	3.37	368	0.006	-31.35	175(β)	178(β)	42.1	$M(-L)\pi \rightarrow (M-L)\pi$
					175(β)	181(β)	35.3	$M(-L)\pi \rightarrow (M-L)\pi$
17	3.57	347	0.013	25.26	174(β)	181(β)	46.0	$M\pi \rightarrow (M-L)\pi$
					174(β)	178(β)	25.3	$M\pi \rightarrow (M-L)\pi$
					171(α)	180(α)	12.1	$M\pi \rightarrow (M-L)\pi$
18	3.59	345	0.006	16.59	172(α)	183(α)	37.8	$M(-L)\pi \rightarrow M\sigma$
					172(α)	177(α)	11.0	$M(-L)\pi \rightarrow (M-L)\pi$
20	3.63	341	0.007	-53.07	175(β)	182(β)	39.2	$M(-L)\pi \rightarrow M-L\pi$
					174(β)	182(β)	28.2	$M\pi \rightarrow M-L\pi$
21	3.67	338	0.002	36.61	164(β)	176(β)	29.1	$L\sigma \rightarrow M\pi$
					174(β)	178(β)	16.6	$M\pi \rightarrow (M-L)\pi$

					174(β)	185(β)	14.5	$M\pi \rightarrow M\sigma$
22	3.73	333	0.030	-9.61	174(β)	182(β)	49.2	$M\pi \rightarrow M-L\pi$
					175(β)	182(β)	14.7	$M(-L)\pi \rightarrow M-L\pi$
23	3.75	330	0.006	-25.21	173(α)	180(α)	58.9	$M(-L)\pi \rightarrow (M-)L\pi$
					173(α)	177(α)	18.1	$M(-L)\pi \rightarrow (M-)L\pi$
26	3.95	314	0.011	15.33	173(α)	179(α)	23.1	$M(-L)\pi \rightarrow L\pi$
					171(α)	184(α)	19.3	$M\pi \rightarrow M\sigma$
					174(β)	186(β)	19.1	$M\pi \rightarrow M\sigma$
					172(α)	177(α)	12.4	$M(-L)\pi \rightarrow (M-)L\pi$
29	4.09	303	0.009	27.19	162(β)	176(β)	57.7	$(M-)L\sigma \rightarrow M\pi$
					171(α)	179(α)	26.6	$M\pi \rightarrow L\pi$
30	4.12	301	0.076	17.00	171(α)	177(α)	48.6	$M\pi \rightarrow (M-)L\pi$
					171(α)	180(α)	18.4	$M\pi \rightarrow (M-)L\pi$
31	4.16	298	0.061	31.34	171(α)	179(α)	28.4	$M\pi \rightarrow L\pi$
					171(α)	184(α)	14.0	$M\pi \rightarrow M\sigma$
					173(α)	179(α)	11.7	$M(-L)\pi \rightarrow L\pi$

^a $M\pi$ = metal-centered π MO (metal-based $d\pi$ orbital)

$M\sigma$ = metal-centered σ MO (metal-based $d\sigma$ orbital)

$L\pi$ = ligand-centered π MO

$M-L\pi$ = metal-ligand-centered π MO

$(M-)L\pi$ = ligand-centered π MO with non-negligible metal $d\pi$ orbital involvement

$M(-L)\pi$ = metal-centered π MO with non-negligible ligand π orbitals involvement

$L\sigma$ = ligand-centered σ MO

$(M-)L\sigma$ = ligand-centered σ MO with non-negligible metal $d\sigma$ orbital involvement

Table S4. Left: Low-energy observed bands and corresponding peak positions in the PES of Ru(acac)₃ (displayed in Figs. 3 and 4, and listed in Table 2). Right: DFT (LC-PBE0*//TZVP) eigenvalues and corresponding molecular orbital (MO) attribution (not in direct connection to the observed bands).

Band	Peak position / eV	E / eV	spin-no.MO / symmetry	Assignment
X	7.10	-6.575	β -175 / a	
		-6.852	β -174 / a	
		-6.888	α -173 / a	Ru 4d _{π}
		-7.120	α -172 / b	
		-7.250	α -171 / a	
		-7.619	β -170 / b	
		-7.728	α -169 / b	acac π
A	8.32	-7.860	β -168 / b	
		-7.933	β -167 / a	acac π / Ru 4d _{π}
		-8.104	α -166 / a	
		-8.547	β -165 / b	
B	9.05	-8.563	α -164 / b	acac σ (C-C) and π (O)
		-8.569	α -163 / b	Ru 4d / acac π (O)
		-9.077	β -162 / a	
C	9.59	-9.145	α -161 / a	
		-9.174	β -160 / b	acac σ (C-C) and π (O)
		-9.330	α -159 / b	
		-9.916	β -158 / a	
		-9.950	β -157 / b	
D	10.41	-10.005	α -156 / a	
		-10.096	β -155 / a	acac σ (C-C), σ (C-H) and π (O)
		-10.143	α -154 / b	
		-10.155	α -153 / a	

D. References

- ¹ TURBOMOLE V6.5 2013, a development of University of Karlsruhe and Forschungszentrum Karlsruhe GmbH, 1989-2007, TURBOMOLE GmbH, since 2007; available from <http://www.turbomole.com>.
- ² R. Ahlrichs, M. Bär, M. Häser, H. Horn, C. Kölmel, *Chem. Phys. Lett.* **1989**, *162*, 165-169.
- ³ F. Furche, R. Ahlrichs, C. Hättig, W. Klopper, M. Sierka, F. Weigend, *WIREs Comput. Mol. Sci.* **2014**, *4*, 91-100.
- ⁴ C. Lee, W. Yang, R. G. Parr, *Phys. Rev. B* **1988**, *37*, 785-789.
- ⁵ A. D. Becke, *J. Chem. Phys.* **1993**, *98*, 5648-5652.
- ⁶ P. J. Stephens, F. J. Devlin, C. F. Chabalowski, M. J. Frisch, *J. Phys. Chem.* **1994**, *98*, 11623-11627.
- ⁷ F. Weigend, R. Ahlrichs, *Phys. Chem. Chem. Phys.* **2005**, *7*, 3297-3305.
- ⁸ D. Andrae, U. Häussermann, M. Dolg, H. Stoll, H. Preuss, *Theoret. Chim. Acta* **1990**, *77*, 123-141.
- ⁹ J. Tomasi, B. Mennucci, R. Cammi, *Chem. Rev.* **2005**, *105*, 2999-3093
- ¹⁰ A. Klamt, G. J. Schüürmann, *J. Chem. Soc., Perkin Trans. 2* **1993**, 799-805.
- ¹¹ M. Cortijo, C. Viala, T. Reynaldo, L. Favereau, I. Fabing, M. Srebro-Hooper, J. Autschbach, N. Ratel-Ramond, J. Crassous, J. Bonvoisin, *Synthesis, Inorg. Chem.* **2017**, *56*, 4555-4567.
- ¹² C. Adamo, V. Barone, *J. Chem. Phys.* **1999**, *110*, 6158-6170.
- ¹³ M. Ernzerhof, G. E. Scuseria, *J. Chem. Phys.* **1999**, *110*, 5029-5036.
- ¹⁴ M. A. Rohrdanz, J. M. Herbert, *J. Chem. Phys.* **2008**, *129*, 034107.
- ¹⁵ R. Baer, E. Livshits, U. Salzner, *Annu. Rev. Phys. Chem.* **2010**, *61*, 85-109.
- ¹⁶ J. Autschbach, M. Srebro, *Acc. Chem. Res.* **2014**, *47*, 2592-2602.
- ¹⁷ M. Srebro, J. Autschbach, *J. Chem. Theory Comput.* **2012**, *8*, 245-256.
- ¹⁸ S. Refaelly-Abramson, S. Sharifzadeh, N. Govind, J. Autschbach, J. B. Neaton, R. Baer, L. Kronik, *Phys. Rev. Lett.* **2012**, *109*, 226405.
- ¹⁹ D. A. Egger, S. Weissman, S. Refaelly-Abramson, S. Sharifzadeh, M. Dauth, R. Baer, S. Kümmel, J. B. Neaton, E. Zojer, L. Kronik, *J. Chem. Theory Comput.* **2014**, *10*, 1934-1952.
- ²⁰ R. van Leeuwen, E. J. Baerends, *Phys. Rev. A* **1994**, *49*, 2421-2431.
- ²¹ Gaussian 09, Revision D.01, M. J. Frisch, G. W. Trucks, H. B. Schlegel, G. E. Scuseria, M. A. Robb, J. R. Cheeseman, G. Scalmani, V. Barone, B. Mennucci, G. A. Petersson, H. Nakatsuji, M. Caricato, X. Li, H. P. Hratchian, A. F. Izmaylov, J. Bloino, G. Zheng, J. L. Sonnenberg, M. Hada, M. Ehara, K. Toyota, R. Fukuda, J. Hasegawa, M. Ishida, T. Nakajima, Y. Honda, O. Kitao, H. Nakai, T. Vreven, J. A. Montgomery, Jr., J. E. Peralta, F. Ogliaro, M. Bearpark, J. J. Heyd, E. Brothers, K. N. Kudin, V. N. Staroverov, R. Kobayashi, J. Normand, K. Raghavachari, A. Rendell, J. C. Burant, S. S. Iyengar, J. Tomasi, M. Cossi, N. Rega, J. M. Millam, M. Klene, J. E. Knox, J. B. Cross, V. Bakken, C. Adamo, J. Jaramillo, R. Gomperts, R. E. Stratmann, O. Yazyev, A. J. Austin, R. Cammi, C. Pomelli, J. W. Ochterski, R. L. Martin, K. Morokuma, V. G. Zakrzewski, G. A. Voth, P. Salvador, J. J. Dannenberg, S. Dapprich, A.

D. Daniels, Ö. Farkas, J. B. Foresman, J. V. Ortiz, J. Cioslowski, and D. J. Fox, Gaussian, Inc., Wallingford CT, 2009.

²² A. Klamt, *J. Phys. Chem.* **1996**, *100*, 3349-3353.

²³ M. Cossi, V. Barone, *J. Chem. Phys.* **2001**, *115*, 4708-4717.

²⁴ Z. Li, W. Liu, *J. Chem. Theory Comput.* **2016**, *12*, 238-260.

²⁵ Z. Li, W. Liu, *J. Chem. Theory Comput.* **2016**, *12*, 2517-2527.

²⁶ I. Tamm, *J. Phys. USSR* **1945**, *9*, 449.

²⁷ S. M. Dancoff, *Phys. Rev.* **1950**, *78*, 382.

²⁸ S. Hirata, M. Head-Gordon, *Chem. Phys. Lett.* **1999**, *314*, 291-299.

²⁹ J. Autschbach, T. Ziegler, S. J. A. van Gisbergen, E. J. Baerends, *J. Chem. Phys.* **2002**, *116*, 6930-6940.

³⁰ J. Bonvoisin, I. Ciofini, *Dalton Trans.* **2013**, *42*, 7943-7951.

³¹ G. A. Garcia, B. K. C. de Miranda, M. Tia, S. Daly, L. Nahon, DELICIOUS III: A multipurpose double imaging particle coincidence spectrometer for gas phase vacuum ultraviolet photodynamics studies. *Rev. Sci. Instrum.* **2013**, *84*, 053112.